Article

Redox-Mediated Synthesis and Encapsulation of Inorganic Nanoparticles in Shell-Cross-Linked Cylindrical Polyferrocenylsilane Block Copolymer Micelles

Hai Wang, Xiaosong Wang, Mitchell A. Winnik, and Ian Manners

J. Am. Chem. Soc., **2008**, 130 (39), 12921-12930 • DOI: 10.1021/ja8028558 • Publication Date (Web): 03 September 2008

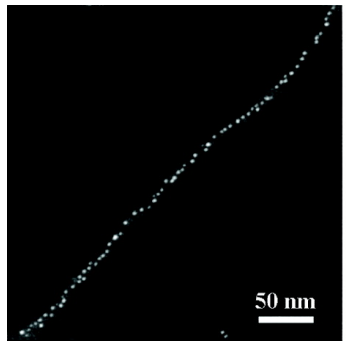

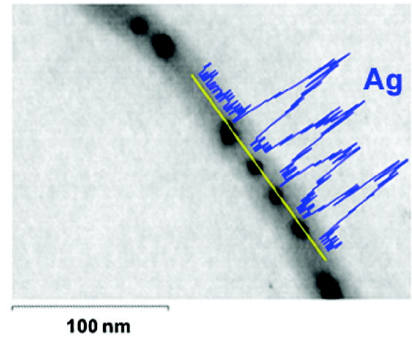

More About This Article

Additional resources and features associated with this article are available within the HTML version:

- Supporting Information
- Access to high resolution figures
- Links to articles and content related to this article
- Copyright permission to reproduce figures and/or text from this article

View the Full Text HTML

J|A|C|S
ARTICLES

Published on Web 09/03/2008

Redox-Mediated Synthesis and Encapsulation of Inorganic Nanoparticles in Shell-Cross-Linked Cylindrical Polyferrocenylsilane Block Copolymer Micelles

Hai Wang,[†] Xiaosong Wang,[†,§] Mitchell A. Winnik,*[,†] and Ian Manners*[,†,‡]

Department of Chemistry, University of Toronto, 80 St. George Street, Toronto, Ontario M5S 3H6, Canada, and School of Chemistry, University of Bristol, Bristol BS8 1TS, United Kingdom

Received April 17, 2008; E-mail: mwinnik@chem.utoronto.ca; ian.manners@bristol.ac.uk

Abstract: Detailed studies of a new approach to the synthesis and encapsulation of silver and silver halide nanoparticles inside shell-cross-linked cylindrical block copolymer polyisoprene-*block*-polyferrocenyldimethylsilane (PI-*b*-PFS) micelles (**1**) through in situ redox reactions are reported. The cylindrical nanostructures **1** were prepared by the solution self-assembly of the PI-*b*-PFS diblock copolymer in the PI-selective solvent hexane followed by Pt(0)-catalyzed PI shell-cross-linking hydrosilylation reactions. The partial preoxidation of the swollen PFS core using tris(4-bromophenyl)aminium hexachloroantimonate [*p*-$BrC_6H_4)_3N$][$SbCl_6$] (**2**, Magic Blue) followed by redox reaction between the remaining Fe(II) centers in the PFS core and Ag^+ cations led to the formation of silver nanoparticles. High-resolution scanning transmission electron microscopy images of the resulting peapod structures provided a clear indication that the nanoparticles were encapsulated inside the micelles. The composition of the nanoparticles was analyzed by energy-dispersive X-ray spectroscopy (EDX). By combining the evolution of the UV−vis spectra of the reaction mixture and EDX measurements, we surprisingly found that silver halide seed particles were formed through a precipitation reaction at an early stage of the encapsulation process. The size of the silver nanoparticles varied with different amounts of silver ions added to the micelle solution. When I_2 was used as the preoxidant, AgI nanoparticles were formed and encapsulated inside the cylinders through the precipitation reaction between iodide anions and silver ions. The packing density of the resulting AgI nanoparticles was increased by an iterative addition method, which utilizes the reversible redox properties of PFS. The small encapsulated AgI nanoparticles were also shown to serve as seeds for the formation of larger Ag nanoparticles when a silver salt was subsequently added.

Introduction

Recently, one-dimensional (1D) nanostructures such as nanowires and arrays of nanoparticles have attracted a great deal of attention because of their unique electronic and optical properties.[1−4] A number of advanced nanolithographic techniques have been developed to synthesize 1D nanostructures such as electron-beam writing,[5] focused ion beam (FIB) lithography,[6] and dip-pen nanolithography (DPN).[7] However, the demanding setup and high cost associated with these techniques has led to interest in other approaches which may complement or possess advantages over these technologies.[8,9] Self-assembly methods may provide a fascinating alternative, and various methods have been explored in the chemical synthesis of 1D nanostructures.[10] As one category of these techniques, template-directed synthesis is one of the most commonly used methods owing to its relative simplicity and easy control of morphology. Among the materials that can be used as building blocks for templating systems, block copolymers that can self-assemble in solution to form elongated structures are of particular interest, considering that the resulting 1D nanostructures can be easily manipulated and processed in the solution phase.

A wide variety of different research groups have recently demonstrated that nonspherical structures such as cylinders and nanotubes can be prepared from block copolymers in either aqueous solutions or organic solvents.[11−26] Generally, templating of metal nanoparticles or other semiconductor particles by polymeric micelles involves two steps: binding of metal ions onto polymer chains via electrostatic interaction or coordination,

[†] University of Toronto.
[‡] University of Bristol.
[§] Present address: Department of Colour Science, School of Chemistry, University of Leeds LS2 9JT, UK.

(1) Alivisatos, A. P. *Science* **1996**, *271*, 933.
(2) Hu, J. T.; Odom, T. W.; Lieber, C. M. *Acc. Chem. Res.* **1999**, *32*, 435.
(3) Barnes, W. L.; Dereux, A.; Ebbesen, T. W. *Nature* **2003**, *424*, 824.
(4) Wang, Z. L. *Adv. Mater.* **2000**, *12*, 1295.
(5) Gibson, J. M. *Phys. Today* **1997**, *50*, 56.
(6) Matsui, S.; Ochiai, Y. *Nanotechnology* **1996**, *7*, 247.
(7) Su, M.; Liu, X. G.; Li, S. Y.; Dravid, V. P.; Mirkin, C. A. *J. Am. Chem. Soc.* **2002**, *124*, 1560.
(8) Mao, C. B.; Solis, D. J.; Reiss, B. D.; Kottmann, S. T.; Sweeney, R. Y.; Hayhurst, A.; Georgiou, G.; Iverson, B.; Belcher, A. M. *Science* **2004**, *303*, 213.
(9) Dujardin, E.; Peet, C.; Stubbs, G.; Culver, J. N.; Mann, S. *Nano Lett.* **2003**, *3*, 413.
(10) Xia, Y. N.; Yang, P. D.; Sun, Y. G.; Wu, Y. Y.; Mayers, B.; Gates, B.; Yin, Y. D.; Kim, F.; Yan, Y. Q. *Adv. Mater.* **2003**, *15*, 353.

followed by reduction or other post-treatments.[27−30] In order to produce spatially organized 1D arrays of particles instead of randomly located ones, micelles with an effective void space inside the core would be ideal. This is similar to the case where carbon nanotubes have been used as templates to encapsulate guest materials, such as ionic species,[31] organic molecules,[32] and metal nanoparticles.[33] In this regard, polymeric nanotubes with interior carboxylic acid groups and impregnatation of these nanostructures with Fe(II)[34] and Pd(II)[35,36] ions have been reported. The Fe^{2+}-containing nanotubes were transformed to polymer/γ-Fe_2O_3 nanofibers after a post-treatment involving the oxidation of Fe(II) by hydrogen peroxide, whereas polymer/Pd hybrid fibers were obtained by reducing Pd(II) using sodium borohydride. More recently, worm-shaped micelles containing CdS quantum dots within the core have been prepared by a two-step process where Cd^{2+} ions were first localized along the core and then H_2S gas was bubbled through the solution to mineralize the Cd^{2+} ions.[37] The core-forming block for these two examples was poly(acrylic acid), which was used to bind the respective metal ions prior to post-treatments. Alternatively, 1D chains of gold nanoparticles have been prepared by triggering a sphere-to-string transition of cross-linked polystyrene-*block*-poly(acrylic acid) micelles with citrate-stabilized Au nanoparticles encapsulated in the core.[38]

We recently described the synthesis of shell-cross-linked organometallic nanotubes that contain a polyferrocenyldimethylsilane (PFS) inner wall covered by a cross-linked network of polymethylvinylsiloxane (PMVS) as a shell.[39] These structures were prepared through a solution self-assembly of PFS-*b*-PMVS block copolymers in hexane, a selective solvent for PMVS, followed by a Pt(0)-catalyzed hydrosilylation to cross-link the PMVS shell. After shell-cross-linking, these polymeric micellar structures are robust and can be manipulated in a variety of organic solvents, including common solvents for both blocks, which greatly facilitates their potential utility in templating novel 1D nanostructures.[40−46] A key characteristic of these structures is that the presence of the PFS core makes them redox-active.[47,48] We have briefly reported our preliminary results which have shown that the Fe(II) sites in the PFS domains of the PFS-*b*-PMVS nanotubes can reduce metal ions such as Ag^+ to the corresponding metals to create 1D arrays of silver nanoparticles within the core.[49] In this process the PFS-*b*-PMVS micelles have a dual function, acting as a reducing agent for silver ions and also serving as a template for the resulting arrays of nanoparticles. The preliminary results suggested that the in situ redox chemistry method provides promising control and regulation of silver nanoparticle formation and therefore complements other approaches.[50]

In recent publications we have also reported the synthesis and characterization of shell-cross-linked PI-*b*-PFS cylinders. The approach was similar to that for PFS-*b*-PMVS nanotubes: self-assembly to form cylindrical micelles with a PFS core and a PI corona followed by Pt-catalyzed hydrosilylative cross-linking of the coronal PI block.[45,51] In a common solvent, swelling of the redox-active PFS core would be expected to create an effective void space for nanoparticle encapsulation, leading to the anticipation of strong analogies with the aforementioned nanotubes. Herein we report the full details of our exploration of the use of the redox-mediated synthesis and encapsulation approach to synthesize 1D arrays of silver and silver halide nanoparticles in shell-cross-linked PI-*b*-PFS cylindrical micelles. Our studies demonstrate that this promising

(11) Price, C. *Pure Appl. Chem.* **1983**, *55*, 1563.
(12) Zhang, L. F.; Eisenberg, A. *Science* **1995**, *268*, 1728.
(13) Yu, K.; Zhang, L. F.; Eisenberg, A. *Langmuir* **1996**, *12*, 5980.
(14) Tao, J.; Stewart, S.; Liu, G. J.; Yang, M. L. *Macromolecules* **1997**, *30*, 2738.
(15) Stewart, S.; Liu, G. *Angew. Chem., Int. Ed.* **2000**, *39*, 340.
(16) Antonietti, M.; Heinz, S.; Schmidt, M.; Rosenauer, C. *Macromolecules* **1994**, *27*, 3276.
(17) Spatz, J. P.; Mossmer, S.; Möller, M. *Angew. Chem., Int. Ed.* **1996**, *35*, 1510.
(18) Won, Y. Y.; Davis, H. T.; Bates, F. S. *Science* **1999**, *283*, 960.
(19) Dalhaimer, P.; Bates, F. S.; Discher, D. E. *Macromolecules* **2003**, *36*, 6873.
(20) Grumelard, J.; Taubert, A.; Meier, W. *Chem. Commun.* **2004**, 1462.
(21) Massey, J.; Power, K. N.; Manners, I.; Winnik, M. A. *J. Am. Chem. Soc.* **1998**, *120*, 9533.
(22) Raez, J.; Manners, I.; Winnik, M. A. *J. Am. Chem. Soc.* **2002**, *124*, 10381.
(23) (a) LaRue, I.; Adam, M.; da Silva, M.; Sheiko, S. S.; Rubinstein, M. *Macromolecules* **2004**, *37*, 5002. (b) Moughton, A. O.; O'Reilly, R. K. *J. Am. Chem. Soc.* **2008**, *130*, 8714. (c) Zhu, J.; Hayward, R. C. *J. Am. Chem. Soc.* **2008**, *130*, 7496.
(24) Li, Z. B.; Kesselman, E.; Talmon, Y.; Hillmyer, M. A.; Lodge, T. P. *Science* **2004**, *306*, 98.
(25) Wang, X. S.; Guerin, G.; Wang, H.; Wang, Y. S.; Manners, I.; Winnik, M. A. *Science* **2007**, *317*, 644.
(26) Cui, H. G.; Chen, Z. Y.; Zhong, S.; Wooley, K. L.; Pochan, D. J. *Science* **2007**, *317*, 647.
(27) Antonietti, M.; Wenz, E.; Bronstein, L.; Seregina, M. *Adv. Mater.* **1995**, *7*, 1000.
(28) Möller, M.; Spatz, J. P. *Curr. Opin. Colloid Interface Sci.* **1997**, *2*, 177.
(29) Djalali, R.; Li, S. Y.; Schmidt, M. *Macromolecules* **2002**, *35*, 4282.
(30) Zhang, M. F.; Drechsler, M.; Müller, A. H. E. *Chem. Mater.* **2004**, *16*, 537.
(31) Meyer, R. R.; Sloan, J.; Dunin-Borkowski, R. E.; Kirkland, A. I.; Novotny, M. C.; Bailey, S. R.; Hutchison, J. L.; Green, M. L. H. *Science* **2000**, *289*, 1324.
(32) Takenobu, T.; Takano, T.; Shiraishi, M.; Murakami, Y.; Ata, M.; Kataura, H.; Achiba, Y.; Iwasa, Y. *Nat. Mater.* **2003**, *2*, 683.
(33) Yuge, R.; Ichihashi, T.; Shimakawa, Y.; Kubo, Y.; Yudasaka, M.; Iijima, S. *Adv. Mater.* **2004**, *16*, 1420.
(34) Yan, X. H.; Liu, G. J.; Liu, F. T.; Tang, B. Z.; Peng, H.; Pakhomov, A. B.; Wong, C. Y. *Angew. Chem., Int. Ed.* **2001**, *40*, 3593.
(35) Li, Z.; Liu, G. J. *Langmuir* **2003**, *19*, 10480.
(36) Yan, X. H.; Liu, G. J.; Haeussler, M.; Tang, B. Z. *Chem. Mater.* **2005**, *17*, 6053.
(37) Duxin, N.; Liu, F. T.; Vali, H.; Eisenberg, A. *J. Am. Chem. Soc.* **2005**, *127*, 10063.
(38) Kang, Y. J.; Erickson, K. J.; Taton, T. A. *J. Am. Chem. Soc.* **2005**, *127*, 13800.
(39) Wang, X. S.; Winnik, M. A.; Manners, I. *Angew. Chem., Int. Ed.* **2004**, *43*, 3703.
(40) Thurmond, K. B.; Kowalewski, T.; Wooley, K. L. *J. Am. Chem. Soc.* **1996**, *118*, 7239.
(41) Huang, H. Y.; Kowalewski, T.; Remsen, E. E.; Gertzmann, R.; Wooley, K. L. *J. Am. Chem. Soc.* **1997**, *119*, 11653.
(42) Qi, K.; Ma, Q. G.; Remsen, E. E.; Clark, C. G.; Wooley, K. L. *J. Am. Chem. Soc.* **2004**, *126*, 6599.
(43) Ding, J. F.; Liu, G. J. *Macromolecules* **1998**, *31*, 6554.
(44) Bütün, V.; Lowe, A. B.; Billingham, N. C.; Armes, S. P. *J. Am. Chem. Soc.* **1999**, *121*, 4288.
(45) Wang, X. S.; Arsenault, A.; Ozin, G. A.; Winnik, M. A.; Manners, I. *J. Am. Chem. Soc.* **2003**, *125*, 12686.
(46) Cao, L.; Manners, I.; Winnik, M. A. *Macromolecules* **2001**, *34*, 3353.
(47) Rulkens, R.; Lough, A. J.; Manners, I.; Lovelace, S. R.; Grant, C.; Geiger, W. E. *J. Am. Chem. Soc.* **1996**, *118*, 12683.
(48) Manners, I. *Chem. Commun.* **1999**, 857.
(49) Wang, X. S.; Wang, H.; Coombs, N.; Winnik, M. A.; Manners, I. *J. Am. Chem. Soc.* **2005**, *127*, 8924.
(50) We note that Shelnutt and co-workers have demonstrated the use of an in situ photocatalytic redox reaction to prepare metal nanowires inside the cavity of porphyrin nanotubes. See, for example: Wang, Z. C.; Medforth, C. J.; Shelnutt, J. A. *J. Am. Chem. Soc.* **2004**, *126*, 16720.
(51) Wang, X. S.; Liu, K.; Arsenault, A. C.; Rider, D. A.; Ozin, G. A.; Winnik, M. A.; Manners, I. *J. Am. Chem. Soc.* **2007**, *129*, 5630.

Scheme 1. Preparation of Shell-Cross-Linked PI-*b*-PFS Micelles (**1**)

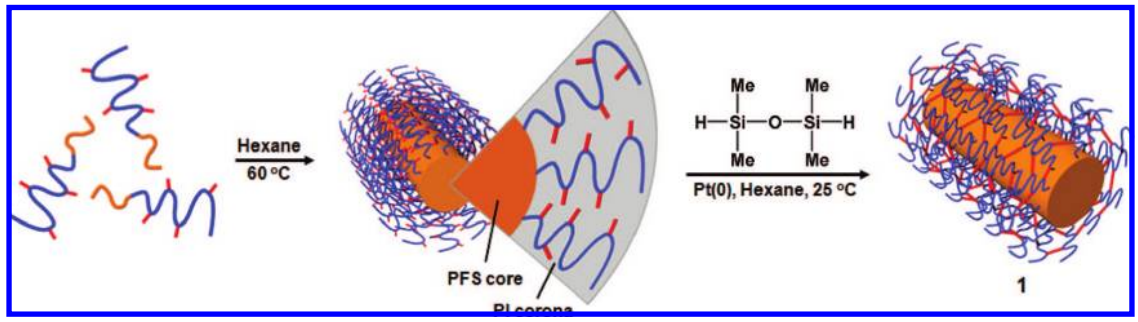

process exhibits important versatility and is also significantly more complex than the simple redox process originally conceived.[52]

Results and Discussion

1. Synthesis and Characterization of Shell-Cross-Linked PI-*b*-PFS Cylinders (1). The synthesis of shell-cross-linked PI-*b*-PFS block copolymer micelles (**1**) used in this study was achieved in three steps. First, the diblock copolymer PI_{320}-*b*-PFS_{55} (the numbers refer to the number average degree of polymerization, M_n = 30 700, PDI = 1.05) was prepared by

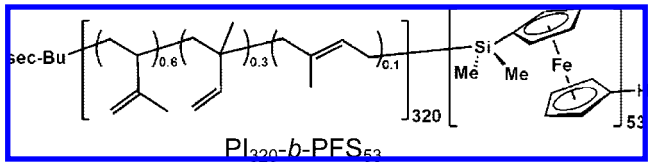

sequential anionic polymerization of isoprene and the appropriate silicon-bridged [1]ferrocenophane.[53] Second, self-assembled cylindrical micelles were prepared in hexane, a selective solvent for PI, by mixing PI_{320}-*b*-PFS_{53} with hexane (1 mg/mL) with stirring at 60 °C for 1 h before cooling to room temperature. An aliquot was taken for transmission electron microscopy (TEM) analysis. Finally, a hydrosilylation reaction catalyzed by Karstedt's catalyst (a 1,3-divinyltetramethyldisiloxane−Pt(0) complex) was performed to cross-link the PI shell of the micelles using tetramethyldisiloxane as the cross-linker (Scheme 1).

The products obtained from the shell-cross-linking reaction were characterized by TEM. Figure 1A presents a TEM image for a sample prepared from an *n*-hexane solution of the micelles after the shell-cross-linking reaction. The micelles seem to be quite rigid and show an average width of 23 nm. When these shell-cross-linked micelles (**1**) were dried and transferred into toluene, a good solvent for both blocks, they maintained their cylindrical structure and uniform width, but they appeared to be more flexible (Figure 1B). Their average width increased to 30 nm.

The effect of shell-cross-linking can be discerned from TEM analysis. Hexane is a selective solvent for PI and a nonsolvent for PFS. The PI-*b*-PFS cylindrical micelles (**1**) were therefore formed and cross-linked in *n*-hexane. Toluene, on the other hand, is a good solvent for both PI and PFS blocks. The non-cross-linked PI-*b*-PFS cylindrical micelles would simply dissociate into unimers in toluene. In contrast, the structures with the PI shell cross-linked as shown in Figure 1B have a well-defined cylindrical shape, analogous to those from *n*-hexane (Figure 1A). This indicates that the covalent linkages in the PI corona formed during the shell-cross-linking reaction effectively locked in the original micellar structures. This greatly increases the processability of PI-*b*-PFS cylindrical micelles.[51] Another feature we noted in these two TEM images is that the width of the micelles from toluene appears to be larger than that of the as-prepared cross-linked micelles from *n*-hexane. The increase in width may be related to the swelling of these micelles in toluene which is due to substrate adhesion effects after the solvent evaporates, or it may be related to flattening of the softer objects on the substrate. The void space created due to the swelling makes it possible to encapsulate guest materials inside the micelles. From this perspective, shell-cross-linked PFS-*b*-PMVS nanotubes and PI-*b*-PFS cylinders (**1**) would be expected to behave similarly.

2. Electrochemical Properties of Shell-Cross-Linked PI-*b*-PFS Micelles (1). The electrochemical properties of **1** were assessed by cyclic voltammetry (CV). The experiments were carried out in a mixture of dichloromethane and benzonitrile (v/v 2:1) with 0.1 M $[Bu_4N][PF_6]$ as the supporting electrolyte. The cyclic voltammogram (Figure 2) showed two reversible oxidation peaks, which were spaced by 0.20 V.[47]

The CV experiment demonstrated that **1** can be reversibly oxidized and reduced. This suggested that an opportunity should exist to repetitively carry out redox reactions using the Fe centers present in the PFS core. In addition, two sets of redox peaks are, on the basis of previous studies of PFS homopolymers,[47,54] indicative of the presence of interacting metal centers that oxidize in two distinct steps. One can also appreciate the fact that the presence of the cross-linked coronal PI in **1** effectively prevented the deposition of oxidized micelles on the electrode. Electrode deposition is typically characterized by a sharp peak upon reduction due to surface-confined redox-active species.[39]

3. Synthesis and Encapsulation of Ag Nanoparticles within Shell-Cross-Linked PI-*b*-PFS Cylindrical Micelles (1). a. Attempted Synthesis by Direct Addition of $Ag[PF_6]$. We initially attempted to synthesize silver nanoparticles inside **1** by adding a toluene solution of $Ag[PF_6]$ dropwise to a micelle solution in toluene (ratio Ag^+:ferrocene units on PFS chains = 1:1). The amount of ferrocene units contained in the solution was determined from the absorbance of the solution measured at 450 nm.[55] The toluene solution of **1** was prepared by adding toluene to a vial containing the solid micelles dried from their hexane solution. During the addition of $Ag[PF_6]$, the reaction mixture changed from light yellow to deep yellow to dark brown in color, and after 30 min a precipitate formed.

(52) For experimental details, refer to the Supporting Information.
(53) Massey, J. A.; Temple, K.; Cao, L.; Rharbi, Y.; Raez, J.; Winnik, M. A.; Manners, I. *J. Am. Chem. Soc.* **2000**, *122*, 11577.
(54) Foucher, D. A.; Honeyman, C. H.; Nelson, J. M.; Tang, B. Z.; Manners, I. *Angew. Chem., Int. Ed.* **1993**, *32*, 1709.
(55) See Supporting Information for further details.

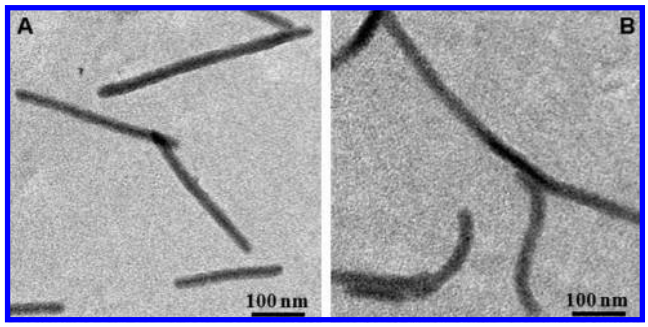

Figure 1. TEM images of shell-cross-linked PI-*b*-PFS micelles (**1**) from (A) *n*-hexane and (B) toluene.

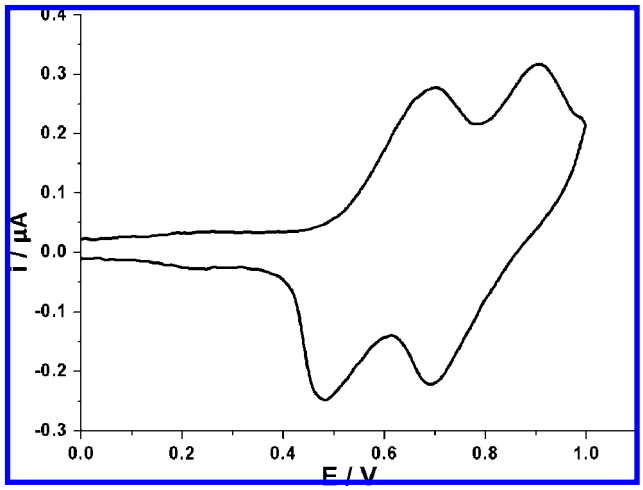

Figure 2. Cyclic voltammogram of **1** in a mixture of dichloromethane and benzonitrile (2:1 v/v) with 0.1 M $[Bu_4N][PF_6]$ as the supporting electrolyte at a scan rate of 25 mV/s. The reference electrode is Ag/AgCl.

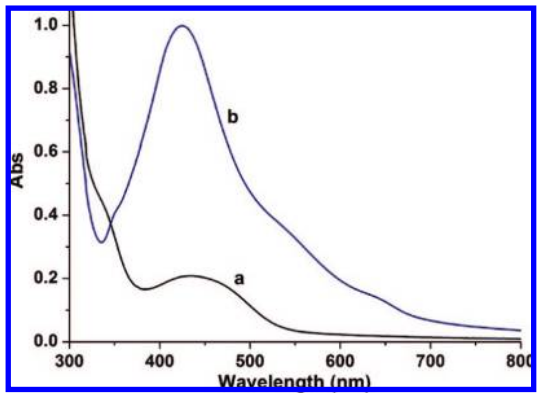

Figure 3. UV−vis spectra of **1** in toluene (a) before and (b) after the addition of $Ag[PF_6]$ (Ag^+:ferrocene units on PFS chains = 1:1).

The reaction was monitored by UV−vis spectroscopy. The spectrum of the starting material, the shell-cross-linked micelles (**1**) in toluene, showed an absorption peak around 450 nm (spectrum a, Figure 3). The spectrum of the reaction mixture taken after the addition of 1 equiv of Ag^+ but before the precipitate was formed showed a weak absorption with a maximum around 630 nm and a very strong absorption band centered at 430 nm (spectrum b, Figure 3).

The difference between these two UV−vis spectra is indicative of the compositional change in the reaction mixture. The distinct absorption band around 450 nm in the absorption spectrum (spectrum a, Figure 3) of **1** is characteristic of unoxidized ferrocene units. After $Ag[PF_6]$ was added, a very strong absorption peak at 430 nm appeared (spectrum b, Figure 3), which we attribute to the surface plasmon resonance absorption of silver nanoparticles.[56] This absorption peak overwhelms the peak at 630 nm arising from the formation of ferrocenium moieties, the oxidized product of ferrocene units. On the basis of these analyses, we infer that, upon addition of $Ag[PF_6]$, Ag^+ ions were reduced to metallic Ag by Fe(II) from PFS with the concomitant formation of ferrocenium centers (eq 1).

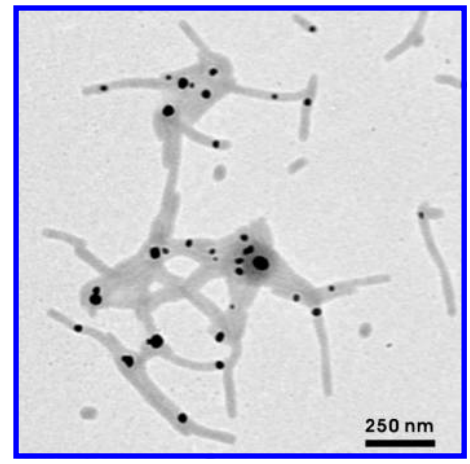

Figure 4. TEM image showing aggregates of **1** with Ag nanoparticles formed outside of the cylinders.

$$Fe^{2+}(PFS) + Ag^+ \rightarrow Fe^{3+}(PFS) + Ag \qquad (1)$$

The precipitate was isolated and characterized by TEM. The TEM sample was prepared by drying a drop of the suspension of the precipitate in toluene on a Formvar and carbon-coated copper grid. One can see that the micelles formed network-like aggregates (Figure 4). The silver nanoparticles of various diameters (ca. 10−50 nm) were randomly located on the micelles, with some bridging different micelles.

From a kinetic point of view, a high local concentration of Fe(II) centers in each micelle might be expected to contribute to the network formation. We hypothesized that a more controlled reaction might take place if the PFS chains were partially preoxidized before $Ag[PF_6]$ was added. The reduced local concentration of Fe(II) centers resulting from the preoxidation would be expected to decrease the rate of the redox process and therefore to be beneficial for the controlled formation of nanoparticles inside the PFS core.

b. Synthesis and Encapsulation of Silver Nanoparticles with Preoxidative Treatment. The reaction to synthesize and encapsulate silver nanoparticles inside PI-*b*-PFS cylinders with preoxidation treatment was carried out in two steps as illustrated in Scheme 2. The pretreatment was first conducted by adding a dichloromethane solution of an organic oxidant, tris(4-bromophenyl)aminium hexachloroantimonate (**2**, also known as Magic Blue), dropwise to a solution of **1** in toluene. The ratio of **2** to the total ferrocene units in **1** was typically no more than 1:4. The color of the reaction mixture turned from light yellow to almost colorless after the pretreatment. A solution of $Ag[PF_6]$ in toluene was then added dropwise.

(56) Kelly, K. L.; Coronado, E.; Zhao, L. L.; Schatz, G. C. *J. Phys. Chem. B* **2003**, *107*, 668.

Scheme 2. Synthesis and Encapsulation of Silver Nanoparticles with Preoxidation Treatment

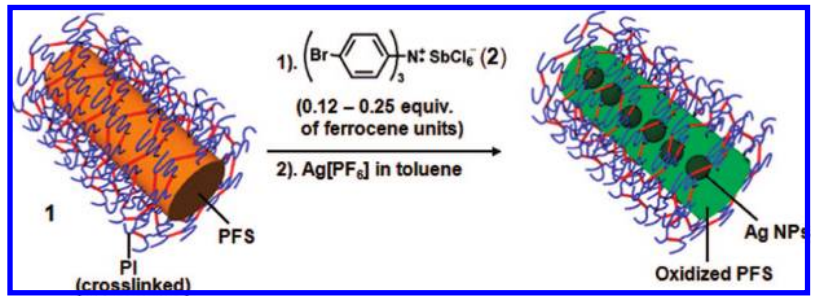

The products from four reactions with different amounts of $Ag[PF_6]$ added were characterized by dark-field TEM. In dark-field TEM, components containing heavy elements scatter more electrons and appear bright against the dark carbon film background. The structures presented in Figure 5 were prepared from **1** pretreated with **2** (0.125 equiv with respect to total ferrocene units), followed by the addition of different amounts of $Ag[PF_6]$. The amount of $Ag[PF_6]$ ranged from 0.125 to 0.75 equiv of total ferrocene units in the solution. When 12.5% $Ag[PF_6]$ was added (note: the percentage hereinafter refers to the mol % of $Ag[PF_6]$ added compared to the total number of ferrocene units in the sample unless stated otherwise), the cylinders encapsulated very small, closely spaced particles ($d \approx 3$ nm) (Figure 5A). When 25% $Ag[PF_6]$ was added, the size of the particles increased ($d = 4.5-5.3$ nm), and the interparticle distance also increased (Figure 5B). The particles appeared to be even larger when the amount of $Ag[PF_6]$ was further increased. The diameter of the particles ranged from 5.3 to 6.6 nm for 50% $Ag[PF_6]$ and from 6.0 to 8.0 nm for 75% $Ag[PF_6]$ (Figure 5C,D).

One can see that the use of **2** as the preoxidant led to most particles in all four samples being positioned nicely along the centerline of PI-*b*-PFS micelles. This strongly suggests that they were encapsulated inside the cylinders. The effect of different amounts of Ag^+ ions added in the encapsulation process can also be identified on the basis of these dark-field TEM images.

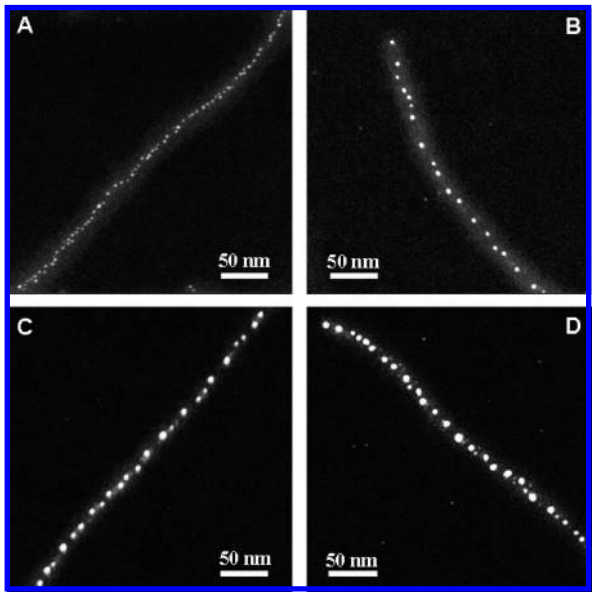

Figure 5. Dark-field TEM images of **1** pretreated with **2** (0.125 equiv of ferrocene units), followed by addition of $Ag[PF_6]$ in different amounts: 12.5% (A), 25% (B), 50% (C), and 75% (D) for total ferrocene units.

The larger the amount of Ag^+ ions added, the larger the encapsulated particles.[57]

The detailed composition of the encapsulated particles was analyzed by energy dispersive X-ray spectroscopy (EDX) operating in line scan and small area scan modes. EDX line scans give elemental constituent changes across a region by scanning the electron beam across an interactively defined line. The term "small area scan" means that the scan area is small comparable to the area occupied by a single particle, typically smaller than 10 × 10 nm. Both of these techniques make it possible to obtain the detailed composition of very small individual nanoparticles.

The results from EDX line scans are presented in Figure 6. Figure 6A shows the EDX profiles along the centerline of a nanoparticle-encapsulated cylinder obtained from **1** with pretreatment with 12.5% of **2** and the addition of 25% $Ag[PF_6]$. From the elemental profiles, we can distinguish three silver signals matching up with the positions of the scanned particles. Surprisingly, we also observed three chlorine signals at the same positions. When 75% $Ag[PF_6]$ was added, the resulting particles gave distinct silver signals corresponding to the positions of the three particles, while chlorine signals were poorly defined (Figure 6B). No other elements involved in the encapsulation process coincide with the patterns of these particles in both cases.

The quantitative analyses of the molar ratio of silver to chlorine for the same samples investigated by dark-field TEM are summarized in Table 1. The composition analyses were computed by software of the Oxford Inca EDX system based on the EDX spectra obtained for each sample, in either the line scan or the small area scan mode. From Table 1, one can see that, with 12.5% $Ag[PF_6]$ added (sample **I**), the molar ratio of Ag to Cl contained in the particles was around 1.6:1. This ratio did not increase significantly for the sample prepared with 25% $Ag[PF_6]$ (sample **II**). For samples **III** and **IV**, this ratio increased markedly with increasing amounts of $Ag[PF_6]$.

To gain more insight into the chemistry occurring in the encapsulation experiments, we measured the UV−vis spectra (Figure 7) for four solutions obtained by adding different amounts of $Ag[PF_6]$ to the preoxidized (12.5%) reaction mixtures in toluene. The solutions used here were the same ones utilized to obtain the TEM images shown in Figure 5 and the EDX analysis in Table 1. All the spectra in Figure 7 were normalized to the same micelle concentration. In the spectrum of the solution with 12.5% $Ag[PF_6]$ added (spectrum b, Figure 7), the peak around 630 nm due to ferrocenium almost overlapped with the one at the same position in the spectrum

(57) Further effort to coalesce the encapsulated particles by using a larger amount of $Ag[PF_6]$ (>75%) was unsuccessful. Instead, we observed free nanoparticles formed outside the micelles by TEM images.

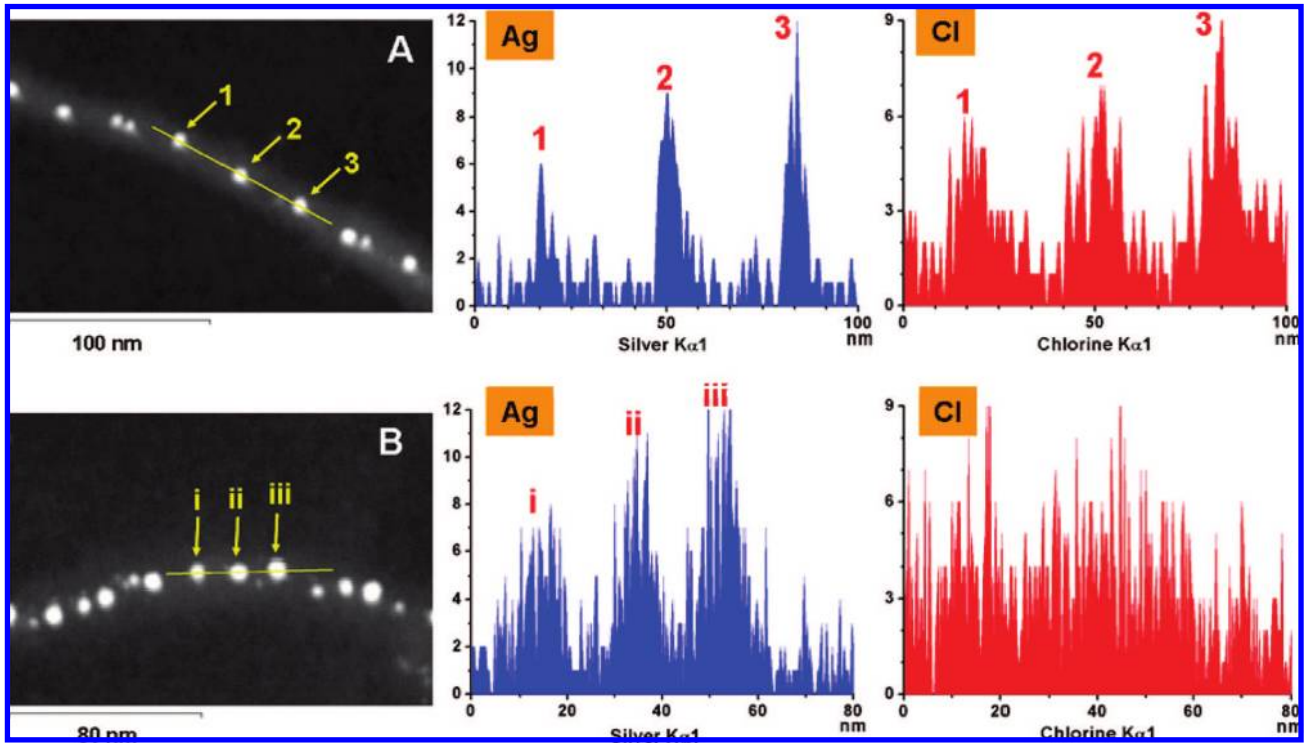

Figure 6. EDX line scan analyses performed along the centerline of a nanoparticle-encapsulated cylinder with (A) 25% and (B) 75% Ag[PF_6] and the corresponding profiles for silver and chlorine. Ag Kα1 and Cl Kα1 counts are plotted as a function of the analysis position on the line.

Table 1. Quantitative Analysis of the EDX Spectra for the Ratio of Silver to Chlorine for the Particles from Four Different Samples

	reagents added (%)[a]		
sample	**2**	Ag[PF_6]	Ag:Cl[b]
I	12.5	12.5	1.6:1
II	12.5	25	1.8:1
III	12.5	50	3.7:1
IV	12.5	75	5.7:1

[a] The amount is relative to the total ferrocene units in each sample. [b] Averaged values based on analyses for ca. 20 particles for each sample.

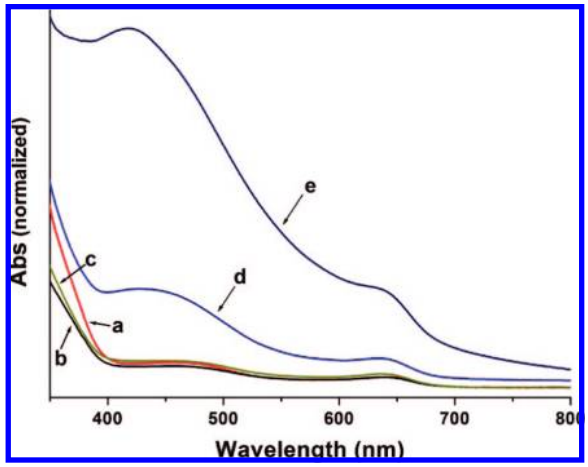

Figure 7. UV−vis spectra of **1** in toluene pretreated with **2** (0.125 equiv per ferrocene unit, a) and followed by the addition of Ag[PF_6] in different amounts: (b) 12.5%, (c) 25%, (d) 50%, and (e) 75% of total ferrocene units. The spectra were normalized to the same concentration.

of the original preoxidized reaction mixture without any Ag[PF_6] (spectrum a, Figure 7). After 25% Ag[PF_6] was added, however, the intensity of the ferrocenium peak at 630 nm increased very slightly (spectrum c, Figure 7). With a further increase in the amount of Ag[PF_6] added (50% and 75%), an intense absorption band centered around 418 nm was detected with the concomitant increase of the peak at 630 nm (spectra d and e, Figure 7).

Since the redox products show characteristic optical absorptions, the information revealed by UV−vis spectroscopy is helpful for identifying species present in the reaction mixtures. The overlap of the ferrocenium peak at 630 nm in the spectra for the preoxidized reaction mixture and the one with 12.5% Ag[PF_6] added indicates that Ag^+ ions added initially did not further oxidize PFS. No additional ferrocenium centers were generated in this step. It is more likely that other non-redox reactions took place. This is somewhat surprising, as we expected added Ag^+ to oxidize PFS. The ferrocenium peak at 630 nm only increased slightly when 25% Ag[PF_6] was added. The intensity of this peak, however, increased significantly when the amount of Ag[PF_6] added was 50% and 75%. In the latter two cases, we also observed a strong absorption peak centered around 418 nm, which can be attributed to the surface plasmon resonance absorption band of silver nanoparticles. This result indicates that Ag nanoparticles formed in these two experiments.

In addition, we found that the amount of **2** added was important for a successful encapsulation experiment. Treatment of **1** with 12.5% and 25% preoxidant (based on total ferrocene) was effective and led to Ag nanoparticles encapsulated inside the cylinders. Our attempts to encapsulate Ag nanoparticles by using a lower degree of preoxidation (5%) failed. No aligned nanoparticles were observed.

c. Mechanism of Ag Nanoparticle Formation. One of the intriguing findings described above is that the particles produced with the Magic Blue (**2**) pretreatment were mainly encapsulated inside the micelles. This result is in sharp contrast to the case where preoxidation with **2** was not performed. Another impor-

tant finding is the detection of chlorine signals in the EDX analyses for the encapsulated particles. It was therefore interesting for us to investigate the mechanism that led to the formation of encapsulated Ag particles and to understand the role of chlorine in the reactions.

We first recall that the addition of 12.5% $Ag[PF_6]$ to a micelle solution pretreated with 12.5% of **2** did not result in an increase in the intensity of the ferrocenium absorption band at 630 nm. Encapsulated small particles (Figure 5A), however, were already formed at this stage. These observations imply that the $Ag[PF_6]$ added did not oxidize PFS. We hypothesized that other types of non-redox reactions were responsible for the formation of these small particles. The EDX analysis for samples obtained from this experiment suggests that the nanoparticles seen in the TEM image were likely AgCl particles.

Increasing the amount of $Ag[PF_6]$ added, however, led to an increase in the intensity of the band at 630 nm. Although the increase was barely observable when 25% $Ag[PF_6]$ was added, it became distinct when 50% and 75% $Ag[PF_6]$ were added. The enhancement of this ferrocenium absorption band indicates the occurrence of the redox reaction between $Ag[PF_6]$ and PFS. Another feature we noted in the latter two cases was the appearance of the strong absorption band centered around 418 nm, which is indicative of the formation of silver nanoparticles.

On the basis of the discussions above, coupled with the fact that the size of the encapsulated nanoparticles increased with an increasing amount of $Ag[PF_6]$, we infer that the encapsulated particles formed via a two-stage pathway. A precipitation reaction occurred first to form AgCl nanoparticles, followed by further reduction of Ag^+ by PFS to form Ag nanoparticles. Support for this idea is provided by the increase of the silver content in the encapsulated particles, as determined by EDX analysis (Table 1).

An important issue to address is the origin of the Cl^- anions. On the basis of the chemicals used in the reactions, the only source that contained chlorine was the $[SbCl_6]^-$ counteranion from the preoxidant **2**. This is not a passive counterion. Cowell et al. reported that $[SbCl_6]^-$ is capable of oxidizing ferrocene to ferrocenium, producing as coproducts complex chlorides of Sb(III) such as $[SbCl_4]^-$, $[Sb_2Cl_9]^{3-}$, or $[SbCl_6]^{3-}$, together with the formation of chloride anions.[58] This led us to suspect that a reaction between $[SbCl_6]^-$ and PFS occurred in our system during the preoxidation step. The resulting chloride anions then reacted with Ag^+ upon the addition of $Ag[PF_6]$, forming AgCl nanoparticles. We believe that the resulting AgCl nanoparticles served as the seeds for the growth of Ag nanoparticles in the second stage.

To determine the amount of chloride anions produced in the preoxidation step in our system, we performed several experiments by adding $Ag[PF_6]$ to micelle solutions in toluene preoxidized with **2** and measured the UV−vis spectra of the solutions. We assumed that the amount of $Ag[PF_6]$ added immediately before the ferrocenium absorption band around 630 nm started increasing should equal the amount of Cl^- in the solution. On the basis of these experiments, we found the averaged molar ratio of chloride anions to **2** to be ca. 1.5:1.

To test the idea that $[SbCl_6]^-$ was necessary for the reactions described above to take place, we conducted a control experiment in which **2** (0.125 equiv of total ferrocene units) was replaced by a different tris(4-bromophenyl)aminium salt, the hexafluorophosphate. The other reaction conditions remained identical. This oxidant has the same radical cation as **2** but a more inert counteranion, $[PF_6]^-$. This is the same counterion contained in the silver salt we used. Here we did not observe an organized 1D array of nanoparticles. Instead, we found that nanoparticles of various sizes (d = 6.5−25.6 nm) formed and were located randomly on the micelles (see Figure S2 in Supporting Information). In addition, a strong absorption band centered at 428 nm was observed in the UV−vis spectra of the reaction mixture upon addition of a small amount of $Ag[PF_6]$.

The results described above suggest that Ag nanoparticles formed right after $Ag[PF_6]$ was added, and these particles were not confined inside the micelles. In contrast, when $[SbCl_6]^-$ was used as the counterion of the preoxidant, the nanoparticles formed initially were AgCl, and they were encapsulated inside the micelles. Thus, the presence of anions that can react with Ag^+ to form a precipitate appears to be necessary in order to encapsulate nanoparticles within the micelles.

We noted that Sen and co-workers have reported a similar approach to synthesize nanoparticles within polymeric materials.[59] The authors used the precipitation reaction between bromide anions and a silver salt to synthesize AgBr nanoparticles. Since the bromide anions were associated with a cationic polymer, the resulting AgBr nanoparticles were embedded in the polymer matrix.

4. Synthesis and Encapsulation of AgI Nanoparticles within Shell-Cross-Linked PI-*b*-PFS Cylindrical Micelles (1). a. Synthesis and Encapsulation of AgI Nanoparticles within 1 Using Iodine as the Oxidant. To expand the scope of our studies, we also explored the synthesis and encapsulation of AgI nanoparticles within PI-*b*-PFS cylindrical micelles. The strategy we employed here was enlightened by the results discussed in the preceeding section. We imagined that, when elemental iodine was utilized as the oxidant,[47] the iodide anions produced should form ion pairs with the ferrocenium centers. These iodide anions could then react with Ag^+ ions to produce AgI nanoparticles confined within the micelles. In this particular case, iodine could serve as the oxidizing agent as well as the source of counteranions.

We performed the encapsulation experiment in two steps, analogous to the method in which **2** was used as the oxidant. First, shell-cross-linked PI-*b*-PFS cylinders (**1**) recovered from evaporation of the solvent of a hexane solution of **1** were transferred into benzene. To this micelle solution, we added a solution of iodine in benzene (I_2:PFS repeat unit = 0.5:1). In the second step, we added a benzene solution of $Ag[PF_6]$ dropwise to the micelle solution with stirring.

The reactions were followed by UV−vis spectroscopy. Spectrum a in Figure 8 is the absorption spectrum of PI-*b*-PFS cylinders in benzene preoxidized by I_2.[60] It displays a strong absorption peak at 360 nm. Upon addition of $Ag[PF_6]$, the intensity of this peak dropped pronouncedly, while the ferrocenium absorption band at 630 nm remained essentially unchanged in intensity. The addition was halted once this 360 nm peak was indistinguishable from the background (spectrum b in Figure 8). At this point, the molar ratio of added $Ag[PF_6]$ to I_2 used in the pretreatment step was approximately 1:1.5.

(58) Cowell, G. W.; Ledwith, A.; White, A. C.; Woods, H. J. *J. Chem. Soc. B* **1970**, 227.

(59) Sambhy, V.; MacBride, M. M.; Peterson, B. R.; Sen, A. *J. Am. Chem. Soc.* **2006**, *128*, 9798.

(60) For detailed studies of the oxidation of PFS by I_2, see: (a) Rulkens, R.; Resendes, R.; Verma, A.; Manners, I.; Murti, K.; Fossum, E.; Miller, P.; Matyjaszewski, K. *Macromolecules* **1997**, *30*, 8165. (b) Pannell, K. H.; Imshennik, V. I.; Maksimov, Y. V.; Il'ina, M. N.; Sharma, H. K.; Papkov, V. S.; Suzdalev, I. P. *Chem. Mater.* **2005**, *17*, 1844.

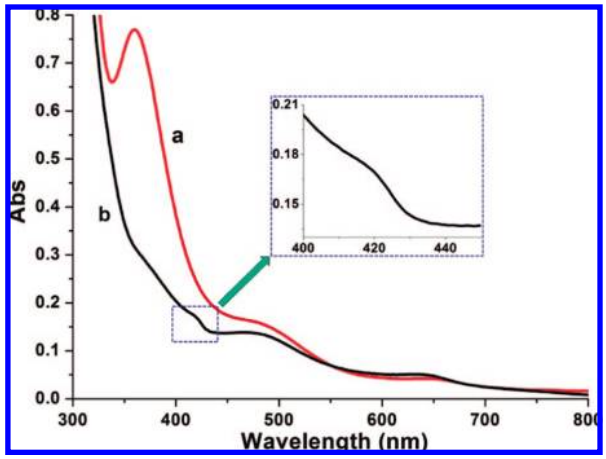

Figure 8. UV−vis spectra of **1** pretreated with I_2 (0.5 equiv of total ferrocene units) before (a) and after (b) the addition of Ag[PF_6] (0.33 equiv of total ferrocene units)).

Close inspection of this UV−vis spectrum revealed a weak absorption band around 420 nm (Figure 8, inset).

The information provided by the UV−vis spectra in Figure 8 can be used to interpret the chemistry that took place during the addition of Ag[PF_6]. The peak around 360 nm is characteristic of triiodide anions.[61] By the time this peak became indiscernible, the molar ratio of added Ag[PF_6] to I_2 reached ca. 1:1.5, which is in a good agreement with the reaction stoichiometry required to form AgI from Ag^+ and I_3^-. Therefore, we believe that the anions produced in the oxidation step were I_3^-. Considering the evolution of the triiodide absorption band and the lack of characteristic surface plasmon resonance absorption of silver nanoparticles, we infer that no redox reaction took place between Ag^+ and I_3^-. Interestingly, a weak absorption band around 420 nm was observed. On the basis of the work of Kimura and co-workers,[62] we infer that the 420 nm peak is due to the surface plasmon resonance absorption of AgI nanoparticles. Abstraction of I^- from I_3^- by Ag^+ might be involved in this precipitation reaction. One might anticipate that the released I_2 may further oxidize the remaining PFS. However, we did not observe an increase in the intensity of the ferrocenium absorption band at 630 nm after Ag[PF_6] was added.

Shown in Figure 9 is a dark-field TEM image of a sample prepared from the resulting solution. One can see that almost all the nanoparticles are located along the centerline of the micelles. The diameters of most of these particles range from 8.4 to 12.5 nm.

The composition of these encapsulated particles was analyzed by EDX. The line scan profiles along the centerline of a cylinder crossing four nanoparticles are shown in Figure 10. The TEM image was taken in the bright-field mode. The elemental profiles for silver and iodine show that the four silver and the four iodine signals are well correlated with the positions of the scanned particles. In addition, a quantitative analysis using the EDX software revealed that the molar ratio of Ag to I is close to 1:1.

On the basis of the UV−vis measurements and the EDX analyses, we infer that the encapsulated nanoparticles are composed of AgI. The successful encapsulation of AgI nanoparticles within **1** again confirms that precipitation reactions can

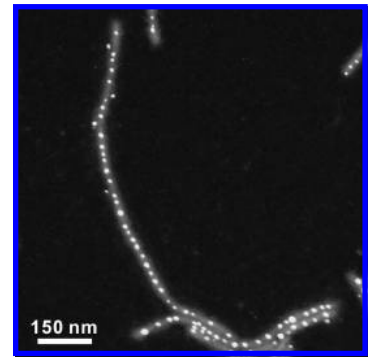

Figure 9. Dark-field TEM image of a sample prepared from I_2-pretreated cross-linked PI-*b*-PFS cylinders (**1**) in benzene after addition of Ag[PF_6].

be highly effective in the formation of nanoparticles confined within a colloidal polymeric host.

b. Iterative Encapsulation of AgI Nanoparticles Utilizing the Reversible Redox Properties of PFS. Since the cyclic voltammogram of **1** showed that these micelles could be reversibly oxidized and reduced, we were attracted by the idea of increasing the density of encapsulated particles or the size of the particles by an iterative encapsulation experiment. Our idea was to perform an encapsulation reaction first and then to reduce the ferrocenium centers produced back to ferrocene units with a reducing agent, and finally to carry out a second encapsulation reaction. Bis(pentamethylcyclopentadienyl)iron(II), Cp^*_2Fe ($Cp^* = \eta$-C_5Me_5), is a suitable reducing agent for our purpose, as it is known to be able to effectively reduce ferrocenium to ferrocene.[63]

We carried out the first encapsulation sequence following the same procedure used to synthesize and encapsulate AgI nanoparticles. I_2 (0.3 equiv of total ferrocene units) was added to a solution of **1** in benzene, followed by the addition of Ag[PF_6]. The ratio of Ag[PF_6] to I_2 was 1:1.5. An aliquot of the reaction mixture was taken for TEM characterization. A solution of decamethylferrocene, Fe(η-C_5Me_5)$_2$ ($FeCp^*_2$), in benzene was then added to the reaction mixture until the ferrocenium peak in the UV−vis spectrum (~630 nm) disappeared. We carried out a second oxidation−precipitation reaction by adding more iodine (I_2 to total ferrocene units= 0.5:1), followed by the addition of Ag[PF_6] (the molar ratio of Ag[PF_6] to I_2 = 1:1.5). The resulting micelles slowly settled to the bottom of the reaction vessel once the stirring was stopped. However, the precipitate was readily redispersed in the solution by agitating the reaction mixture.

The products after the first and second additions of Ag[PF_6] were examined by TEM. Shown in Figure 11A is a dark-field TEM image of the product obtained from the first encapsulation experiment. One sees that the resulting nanoparticles are located along the centerlines of the cylinders. After the second oxidation−precipitation reaction, the cylinders seen in Figure 11B have more particles densely packed along their centerlines, with many small particles present between the large particles. In addition, the interparticle distance is significantly reduced, often to less than 5 nm. A few particles, including some large nanoparticles (d = 6.2−8.9 nm), can be seen outside the micelles.

A shoulder-type absorption band at ca. 420 nm, characteristic of AgI nanoparticles, was observed in the UV−vis spectra of

(61) Salman, H. M. A.; Mahmoud, M. R.; Abou-El-Wafa, M. H. M.; Rabie, U. M.; Crabtree, R. H. *Inorg. Chem. Commun.* **2004**, *7*, 1209.
(62) Chen, S. H.; Ida, T.; Kimura, K. *J. Phys. Chem. B* **1998**, *102*, 6169.
(63) Connelly, N. G.; Geiger, W. E. *Chem. Rev.* **1996**, *96*, 877.

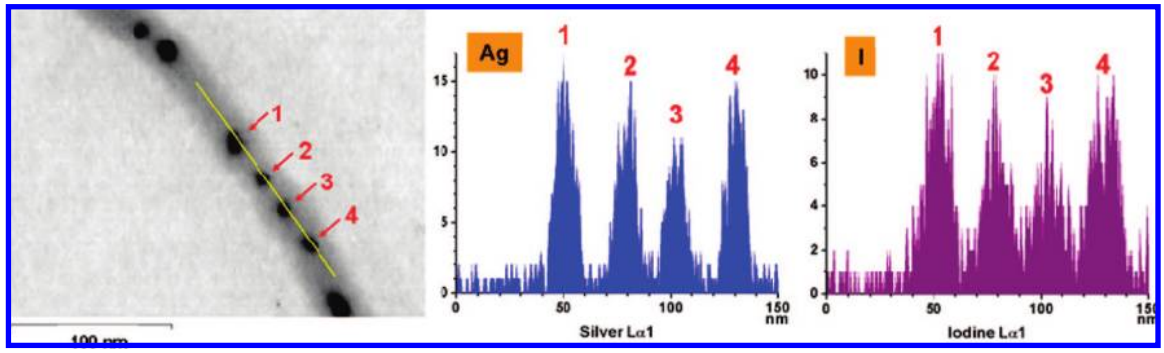

Figure 10. EDX line scan analysis performed along the centerline of a nanoparticle-encapsulated cylinder and elemental profiles for silver and iodine. Ag Lα1 and I Lα1 counts are plotted as a function of the analysis position on the line.

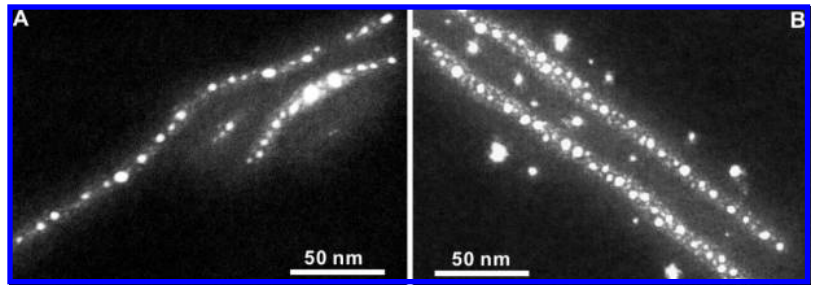

Figure 11. Dark-field TEM images show AgI nanoparticles encapsulated in **1** after (A) the first encapsulation process (the molar ratio of added $Ag[PF_6]$ to total ferrocene units = 1:5) and (B) the second encapsulation process (the molar ratio of added $Ag[PF_6]$ to total ferrocene units = 1:3).

the reaction mixture after the first and second additions of $Ag[PF_6]$. Surface plasmon resonance absorption of Ag nanoparticles, however, was not discernible. We therefore infer that the particles formed in both cases were AgI.

The results presented above clearly support our concept of using the reversible redox properties of PFS to increase nanoparticle packing density inside the micelles. Although the particles formed after the iterative addition experiment are not as well-aligned as those obtained from the first step, they still appear to be along the central part of cylinders. We infer that they were still encapsulated inside the shell-cross-linked PI-*b*-PFS cylindrical micelles (**1**).

c. Using Iodine as the Preoxidant To Synthesize and Encapsulate Ag Nanoparticles within Shell-Cross-Linked PI-*b*-PFS Cylinders (1). To test the idea whether I_2 could behave similarly to **2** as a preoxidant in producing Ag nanoparticles, we performed an experiment in which shell-cross-linked PI-*b*-PFS cylinders (**1**) were first preoxidized to a low degree by I_2, followed by the addition of a larger amount of $Ag[PF_6]$. The amount of I_2 added for preoxidation was 0.15 equiv of total ferrocene units.[64] The molar ratio of $Ag[PF_6]$ to total ferrocene units was 0.6:1. After the amount of added $Ag[PF_6]$ reached 0.1 equiv of total ferrocene units in the sample, a UV−vis spectrum was taken for the reaction mixture. A TEM sample of this reaction mixture was also prepared for later studies. After the second portion of $Ag[PF_6]$ was added (0.5 equiv of total ferrocene units), UV−vis spectroscopy and TEM were also used to characterize the product.

Figure 12A shows the UV−vis spectra measured for the reaction mixture at the two different reaction stages. We can see that, when the ratio of $Ag[PF_6]$ to total ferrocene units reached 1:10 (the molar ratio of $Ag[PF_6]$ to I_2 = 1:1.5), a weak absorption band around 422 nm is discernible (spectrum I in Figure 12A, inset), while the strong peak around 360 nm disappears. This spectrum is similar to spectrum b in Figure 8. After all the $Ag[PF_6]$ was added (0.6 equiv of total ferrocene units), a strong broad absorption peak centered around 420 nm was detected (spectrum II in Figure 12A), and the ferrocenium absorption peak around 630 nm increased significantly.

In Figure 12B, we show a dark-field TEM image for a sample prepared after a small amount of $Ag[PF_6]$ was added (0.1 equiv of ferrocene units). One sees that nanoparticles formed along the centerline of the cylinder. Many small particles ($d \approx 2.0$ nm) were located between relatively large ones ($d \approx 5.0$ nm). After all the $Ag[PF_6]$ (a total of 0.6 equiv of ferrocene units) was added, the nanoparticles along the two parallel micelles in Figure 12C appeared to be much larger ($d \approx 14$ nm) and were spaced farther apart.

The difference in the UV−vis absorption spectra seen in Figure 12 reveals the compositional change of the resulting nanoparticles. After the first part of $Ag[PF_6]$ was added, a weak shoulder at 422 nm can be observed. The appearance of this absorption band is characteristic for AgI nanoparticles and suggests that the particles shown in Figure 12B are AgI. After all the $Ag[PF_6]$ was added, an intense broad absorption peak around 420 nm was detected. This peak can be attributed to the surface plasmon resonance absorption of Ag nanoparticles. EDX analyses for individual particles from this sample confirmed that the resulting nanoparticles were composed of silver and iodine with an average molar ratio of ca. 2.6:1. We therefore conclude that the AgI nanoparticles formed initially also served as the seeds for the growth of Ag nanoparticles.

Summary

We fabricated one-dimensional arrays of Ag nanoparticles within shell-cross-linked cylindrical PI-*b*-PFS block copolymer micelles (**1**) using an in situ redox reaction between the

(64) This is slightly larger, on a mole equivalent basis, than the amount of **2** used in the reactions described above.

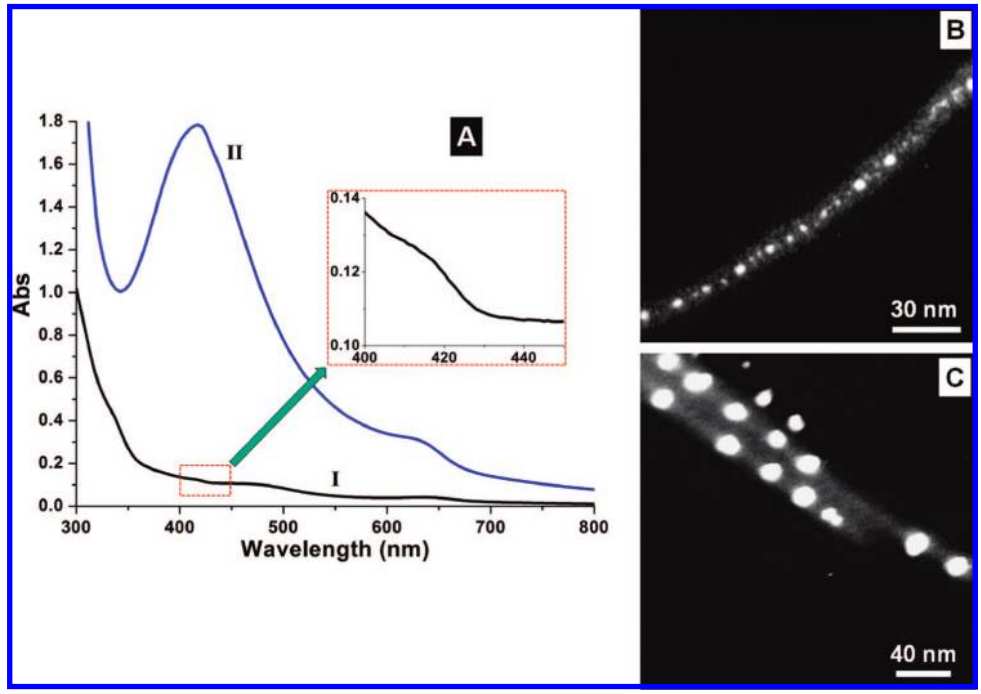

Figure 12. Two samples were prepared from **1** preoxidized with I_2 (0.15 equiv of total ferrocene units), followed by the sequential addition of two different amounts of $Ag[PF_6]$. Sample **a** was obtained after the first portion of $Ag[PF_6]$ was added (0.1 equiv relative to total ferrocene units). Sample **b** was obtained after an additional amount of $Ag[PF_6]$ was added (a total of 0.6 equiv relative to total ferrocene units). (A) UV−vis spectra of sample **a** (I) and sample **b** (II). Dark-field TEM images of sample **a** (B) and sample **b** (C).

electroactive PFS core and silver ions. The shell-cross-linked PI-*b*-PFS cylinders not only acted as a reducing agent for the formation of Ag nanoparticles but also served as templates that directed the resulting particles to arrange in a one-dimensional fashion. The pretreatment of the micelles **1** with organic oxidant **2** was found to be a key step to obtain Ag nanoparticles confined inside the micelles. On the basis of UV−vis measurements and EDX analyses, we proposed a two-step pathway for the formation of Ag nanoparticles, namely a precipitation reaction to form AgCl seed particles followed by reduction of Ag^+ by PFS to yield Ag nanoparticles. The size of the encapsulated particles could be varied by adding different amounts of silver ions to the reaction mixture.

Using elemental iodine as the preoxidant, we also synthesized one-dimensional arrays of AgI nanoparticles. The packing density of the resulting AgI nanoparticles was increased by an iterative encapsulation process. When the amount of iodine added was small, the AgI nanoparticles formed initially also acted as seeds for the growth of Ag nanoparticles. Although the research described here should be regarded as exploratory at this stage, the results are promising. Future generations of the peapod-like hybrid nanostructures that we obtained with Ag, AgCl, AgI, or related nanoparticles in the core may ultimately find their use in the fabrication of nanodevices.[65]

Acknowledgment. The authors thank NSERC Canada for funding. We thank Dr. Neil Coombs for assistance with electron microscopy imaging at the Centre of Nanostructure Imaging, Department of Chemistry, University of Toronto. I.M. thanks the European Union for a Marie Curie Chair and the Royal Society for a Wolfson Research Merit Award. We thank a reviewer for helpful comments on network formation and the role of preoxidation.

Supporting Information Available: Experimental details for the synthetic work. This material is available free of charge via the Internet at http://pubs.acs.org.

JA8028558

(65) Warner, M. G.; Hutchison, J. E. *Nat. Mater.* **2003**, *2*, 272.